First-principles investigation of the composition dependent properties of $Ni_{2+x}Mn_{1-x}Ga$ shape-memory alloys

Chun-Mei Li,[1,2] Hu-Bin Luo,[1] Qing-Miao Hu,[1,2,*] Rui Yang,[1] Börje Johansson,[2,3,4] and Levente Vitos[2,3,5]
[1]*Shenyang National Laboratory for Materials Science, Institute of Metal Research, Chinese Academy of Sciences, 72 Wenhua Road, Shenyang 110016, China*
[2]*Applied Materials Physics, Department of Materials Science and Engineering, Royal Institute of Technology, Stockholm SE-100 44, Sweden*
[3]*Condensed Matter Theory Group, Physics Department, Uppsala University, Uppsala SE-75121, Sweden*
[4]*School of Physics and Optoelectronic Technology & College of Advanced Science and Technology, Dalian University of Technology, Dalian 116024, China*
[5]*Research Institute for Solid State Physics and Optics, P.O. Box 49, Budapest H-1525, Hungary*
(Received 7 January 2010; revised manuscript received 11 June 2010; published 7 July 2010)

The composition dependent lattice parameter, phase stability, elastic moduli, and magnetic transition temperature of the $Ni_{2+x}Mn_{1-x}Ga$ shape-memory alloys are studied by using the first-principles exact muffin-tin orbital method in combination with the coherent potential approximation. The lattice parameter and tetragonal shear modulus of the cubic $L2_1$ austenite phase decreases linearly with increasing concentration x of excess Ni atoms. The heats of formation of both cubic $L2_1$ and tetragonal β''' phases and their difference increase with x, indicating decreasing stability of the cubic and tetragonal phases and increasing driving force for the $L2_1$ to β''' martensitic transition. Investigating the electronic density of states, we find that the Ni-induced decreasing phase stability can mainly be ascribed to the weakening of the covalent bonding between minority spin states of Ni and Ga. Using the computed parameters, the composition dependence of the martensitic transition temperature is discussed. The theoretical Curie temperature, estimated from the Heisenberg model in combination with the mean-field approximation, is larger for the β''' phase than for the $L2_1$ phase. For both phases, the Curie temperature decreases nearly linearly with increasing x.

DOI: 10.1103/PhysRevB.82.024201 PACS number(s): 62.20.fg, 31.15.es, 75.50.Cc, 64.70.kd

I. INTRODUCTION

Due to the indirect exchange interaction between Mn ions, Ni_2MnGa is ferromagnetic (FM) with Curie temperature $T_C=376$ K.[1] The stoichiometric Ni_2MnGa undergoes a structural phase transition at temperature $T_M=202$ K from the high-temperature cubic $L2_1$ structure to a martensitic phase with complex tetragonal structure.[1] This martensitic transition (MT) is reversible, resulting in the shape-memory effect in this system.

Upon alloying, both critical temperatures can be sensitively tuned. Different combinations of T_M and T_C result in different properties of the alloys with various technological significances. For example, the T_M and T_C of $Ni_{2+x}Mn_{1-x}Ga$ alloys with x between 0.18 and 0.20 have T_M and T_C close to each other.[2] Consequently, the structural and the magnetic transitions may couple to each other. This coupling makes it possible to achieve shape-memory effect by applying magnetic field and may induce some attractive properties such as giant magnetocaloric effect, magnetostriction, and magnetoresistance which are important for the application of magnetic refrigeration or magnetostrictive transducers.[3–9] With $x>0.3$, T_M is higher than T_C so that the MT occurs in the paramagnetic (PM) region. In this region, T_M increases drastically with x such that $Ni_{2+x}Mn_{1-x}Ga$ with a high Ni excess can be used as a high-temperature shape-memory alloy. To build the connection between the composition and T_M as well as T_C and to understand the underlying physics are critical for designing new Ni-Mn-Ga based alloys with desirable properties.

There are several plausible quantities to connect the composition and T_M of Ni-Mn-Ga based alloys, among which the e/a ratio (the number of valence electrons per atom) is very well recognized. It has been shown that increasing e/a ratio lowers T_M.[10–12] However, such a connection is coarse grained and fails in some situations. For example, replacing Ga by Al or In and varying the long-range atomic order change T_M without altering the e/a ratio.[13–16] The total energy difference (ΔE_{AM}) between the parent austenite and the tetragonal martensite phases is another quantity proposed to correlate T_M with the composition of the alloys.[17,18] It was shown that a larger ΔE_{AM} corresponds to a higher T_M.[17,18] Interestingly, such a relationship also works for other shape-memory alloys such as TiX with X=Ni, Pd, and Pt.[19] Third, the MT of Ni-Mn-Ga alloys results from the soft-phonon modes and their accompanying soft tetragonal shear modulus $C'=\frac{1}{2}(C_{11}-C_{12})$ of the high-temperature parent phase.[20–22] For alloys undergoing MT, the composition dependence of T_M is generally related to the composition dependence of C': the lower the elastic constant, the higher the T_M will be.[23–25] This relationship is confirmed for both TiNi-based shape-memory alloys and various kinds of off-stoichiometric Ni_2MnGa alloys.[21,26,27] Finally, according to Lanska *et al.*[10] and Banik *et al.*,[28] the composition dependent tetragonality of the martensite ($|c/a-1|$), with a and c being the lattice constants of the martensite) may also serve as an index of the composition dependence of T_M, i.e., a larger $|c/a-1|$ corresponds to a higher T_M. Thus, at least four physical quantities have been reported to be relevant to the composition dependence of T_M. It is therefore of fundamental interest to per-

form a systematic investigation of these claimed correlations for a specified alloy and to assess their validity.

Within the Stoner model the magnetic transition temperature may be related to the magnetization energy, i.e., the energy difference between the nonmagnetic and the FM states.[17,29,30] However, in the PM state above T_C the system may possess nonvanishing localmagnetic moments. The PM state may be modeled by the so-called disordered local magnetic moment (DLM) picture.[31] In this case, T_C is estimated from the energy difference between the DLM and the FM states by taking into account the magnetic entropy of the completely disordered paramagnetic phase as suggested by Grimvall.[32] Thus, in principle, the composition dependence of T_C could be established by evaluating the composition dependent magnetic energy. A more advanced description of the magnetic interactions and magnetic-transition temperature is offered by the Heisenberg model. Within the mean-field approximation (MFA), the transition temperature is directly related to the exchange interactions entering the classical Heisenberg Hamiltonian.[33,34] The transition temperature of Ni_2MnGa alloy from the Heisenberg model was found to be rather close to the experimental value.[35] However, to our knowledge, no theoretical determination of the composition dependence of T_C for $Ni_{2+x}Mn_{1-x}Ga$ using the Heisenberg model has yet been performed.

The purpose of this paper is to study the above-mentioned quantities using first-principles alloy theory and investigate their correlation with the measured T_M and T_C data. In particular, we calculate the composition dependence of the e/a ratio, the energy difference between the austenite and martensite phases, the tetragonal shear modulus C' for the austenite phase, the tetragonality $|c/a-1|$, and the magnetic interactions. $Ni_{2+x}Mn_{1-x}Ga$ alloy is a perfect protocol for such a purpose since the composition dependence of T_M and T_C is available from experiments. The paper is arranged as follows: in Sec. II, we describe the employed first-principles method and the details of the calculations. In Sec. III, the composition dependent properties of $Ni_{2+x}Mn_{1-x}Ga$ are reported, and their relationships with the experimental martensitic transformation temperature and Curie temperature as well as the electronic origin of the composition dependence are discussed. Finally, we summarize the main results of this work in Sec. IV.

II. METHODOLOGY

A. Calculations details

The first-principles method used in the present work is based on the density-functional theory.[36] Although it has been generally accepted that the full-potential methods describe the solids more accurately, here we employ the exact muffin-tin orbitals (EMTOs) method[37,38] in combination with the optimized overlapping muffin-tin approximation for the effective potential[37,39] and the full-charge density technique for the total energy.[38,40] The motivation for our choice is that the full-potential methods are not flexible enough to describe the random distribution of the Ni atoms on the Mn sublattice and the random distribution of the local magnetic moments in the paramagnetic phase. Within the EMTO method, the single-electron Kohn-Shan equations are solved by the Green's-function technique and the substitutional disorder is treated using the coherent potential approximation (CPA).[41–43]

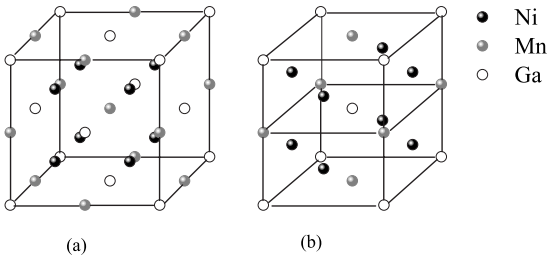

FIG. 1. (a) Unit cells of standard stoichiometric Ni_2MnGa with simple cubic $L2_1$ structure and (b) body-centered-tetragonal structure in the [110] direction.

For the present application, the EMTO basis set included s, p, d, and f components. The Green's function was calculated for 16 complex energy points distributed exponentially on a semicircular contour. We have found that the usual setup of the muffin-tin potential sphere (R_{mt}), $R_{mt}=R_{ws}$ with R_{ws} being the Wigner-Seitz radius, yields larger C' compared to the experiment.[27] Nevertheless, as it is pointed out in Refs. 37–39 the EMTO results can be improved by optimizing the overlapping potential spheres. Therefore, for the present application, after a careful potential optimization, we set $R_{mt}^{Ni}=0.95R_{ws}$ for the atoms on the Ni sublattice and kept all the other R_{mt} equal to R_{ws}. In the one-center expansion of the full-charge density, the number of orbitals was set as 10. The scalar-relativistic and soft-core approximations were adopted. The Ni $3d^84s^2$, Mn $3d^54s^2$, and Ga $3d^{10}4s^24p^1$ were treated as valence states. As we will see later, the soft-core approximation in combination with the *spdf* basis set yields more accurate theoretical lattice constants than the frozen-core approximation and the *spd* basis set.[27] The electronic exchange-correlation potential was described with the generalized-gradient approximation (GGA) by Perdew, Burke, and Ernzerhof (PBE).[44] For comparison, the lattice parameter and elastic modulus of pure Ni_2MnGa were also calculated by using local-spin density approximation (LSDA).[45] The Brillouin zone was sampled by a uniform k-point mesh. We found that a k mesh of $17\times17\times17$ gave well converged total energies for the present systems.

The crystal structure of the high-temperature $L2_1$-Ni_2MnGa austenite is shown in Fig. 1(a). The unit cell is comprised of four interpenetrating fcc lattices A (0, 0, 0), B $(\frac{1}{2},\frac{1}{2},\frac{1}{2})$, C $(\frac{1}{4},\frac{1}{4},\frac{1}{4})$, and D $(\frac{3}{4},\frac{3}{4},\frac{3}{4})$. The Ga and Mn atoms occupy, respectively, the A and B sites, and the Ni atoms occupy the C and D sites. Figure 1(b) depicts the crystal structure of the nonmodulated tetragonal martensite. As reported in a recent study,[27] the excess Ni atoms in $Ni_{2+x}Mn_{1-x}Ga$ prefer to occupy the Mn sublattice. Here we assumed that the excess Ni atoms are distributed randomly on the Mn sublattice. The theoretical phase stability, lattice parameters, and elastic properties were calculated for $x\leq0.2$, and the magnetic interactions for $x\leq0.36$.

B. Calculation of the elastic constants

The equilibrium volume and the bulk modulus of the $L2_1$ austenite phase were determined by fitting the calculated to-

TABLE I. Equilibrium lattice parameter a, bulk modulus B, shear moduli C' and C_{44}, and the total magnetic moment μ_0 of Ni_2MnGa in the $L2_1$ Heusler structure, in comparison with other theoretical and experimental data.

Method	a (Å)	B (GPa)	C' (GPa)	C_{44} (GPa)	$\mu_0(\mu_B)$
This work (GGA-PBE)	5.8208	157.5 ± 0.60	7.9 ± 0.35	107.0 ± 0.69	3.96
This work (LSDA)	5.6563	202.2 ± 0.54	11.7 ± 0.43	134.7 ± 0.37	
EMTO (*spd*, GGA-PBE)[a]	5.8922	151.9	15.9	99.4	4.05
PP[b]	5.8368	151.6	6.3	102.0	4.27
FLAPW[c]	5.8104	156.0			4.09
Experiments	5.8250[d]	146[e],106[f]	4.5[e], 22[f], 6.5[g]	103[e], 102[f], 98[g]	4.17[e]

[a]Reference 27.
[b]References 20 and 49.
[c]Reference 50.
[d]Reference 1.
[e]Reference 51.
[f]Reference 52.
[g]Reference 53.

tal energies versus volume (nine data points) to a Morse function.[46] The elastic moduli C' and C_{44} were calculated by the use of volume conserving orthorhombic and monoclinic deformations, i.e.,

$$\begin{pmatrix} 1+\delta_o & 0 & 0 \\ 0 & 1-\delta_o & 0 \\ 0 & 0 & \dfrac{1}{1-\delta_o^2} \end{pmatrix} \tag{1}$$

and

$$\begin{pmatrix} 1 & \delta_m & 0 \\ \delta_m & 1 & 0 \\ 0 & 0 & \dfrac{1}{1-\delta_m^2} \end{pmatrix}, \tag{2}$$

respectively. Six strains from $\delta=0$ to 0.05 with interval of 0.01 were used to calculate the total energies $E(\delta_o)$ and $E(\delta_m)$. The elastic constants C' and C_{44} were obtained by fitting the total energies with respect to δ_o and δ_m as $E(\delta_o) = E(0) + 2VC'\delta_o^2$ and $E(\delta_m) = E(0) + 2VC_{44}\delta_m^2$, respectively. C_{11} and C_{12} were then evaluated from the bulk modulus $B = \frac{1}{3}(C_{11} + 2C_{12})$ and the tetragonal shear constant $C' = \frac{1}{2}(C_{11} - C_{12})$. Finally, the error bars for the calculated shear elastic constants were obtained from the numerical fit of $E(\delta)$.

C. Calculation of the T_C

The Curie temperature (T_C) of $Ni_{2+x}Mn_{1-x}Ga$ was estimated using the well-established Heisenberg model. According to that, the interatomic exchange interactions are described in terms of the classical Heisenberg Hamiltonian

$$H_{\text{eff}} = -\sum_{\mu,\nu} \sum_{\mathbf{R},\mathbf{R}'} J^{\mu\nu}_{\mathbf{R}\mathbf{R}'} \mathbf{s}^{\mu}_{\mathbf{R}} \mathbf{s}^{\nu}_{\mathbf{R}'}, \quad \mu\mathbf{R} \neq \nu\mathbf{R}', \tag{3}$$

where $J^{\mu\nu}_{\mathbf{R}\mathbf{R}'}$ are the intrasite exchange integrals, the indices μ and ν are 1 and 2, representing the Mn and Ni sublattices, respectively, $\mathbf{R}$ and $\mathbf{R}'$ are the lattice vectors specifying the atoms within sublattices, and $\mathbf{s}^{\mu}_{\mathbf{R}}$ is the unit vector pointing in the direction of the magnetic moment at site $(\mu, \mathbf{R})$.

Within the mean-field solution of the Heisenberg model, T_C is obtained by solving the system of coupled equations[35,47]

$$\langle s^{\mu} \rangle = \frac{2}{3k_B T} \sum_{\nu} J_0^{\mu\nu} \langle s^{\nu} \rangle, \tag{4}$$

where $J_0^{\mu\nu} \equiv \Sigma_{\mathbf{R}} J_{0\mathbf{R}}^{\mu\nu}$ is the effective exchange parameter, and $\langle s^{\nu} \rangle$ is the average z component of $\mathbf{s}^{\nu}_{\mathbf{R}}$. Equation (4) has nontrivial solutions if the corresponding determinant is zero, viz.,

$$Det\{\mathbf{J} - \mathbf{TI}\} = \mathbf{0}, \tag{5}$$

where the matrix elements are $J^{\mu\nu} = (2/3k_B) J_0^{\mu\nu}$ and $I^{\mu\nu} = \delta_{\mu\nu}$ (δ being the Kronecker delta). The largest eigenvalue of Eq. (5) gives the magnetic transition temperature.[35,47] In the present application, the exchange interactions for cubic and tetragonal $Ni_{2+x}Mn_{1-x}Ga$ alloys were calculated using the magnetic force theorem[48] implemented in the EMTO method.[37]

III. RESULTS AND DISCUSSION

A. Properties of cubic Ni_2MnGa

Table I lists the equilibrium lattice parameter a, the bulk modulus B, the shear moduli C' and C_{44}, and the total magnetic moment per unit cell μ_0 cubic Ni_2MnGa. Compared to our previous EMTO calculations reported in Ref. 27, the present lattice constant (5.8208 Å) from GGA-PBE calculation is in better agreement with the experimental value (5.8250 Å) and those from plane-wave pesudopotential[20] as well as full-potential linearized plane-wave[54] calculations. This good agreement is due to the large basis-set and soft-core approximation employed in the present work. Furthermore, with the numerical parameters adopted here, we obtain

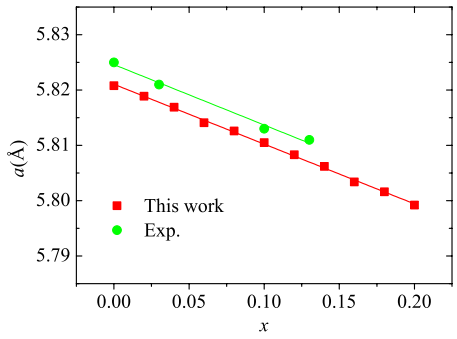

FIG. 2. (Color online) Theoretical equilibrium lattice constants (red squares) of $Ni_{2+x}Mn_{1-x}Ga$ ($x \leq 0.2$) alloys with $L2_1$ structure as a function of the concentration x. For comparison the experimental data are also shown (green circles) (Ref. 28).

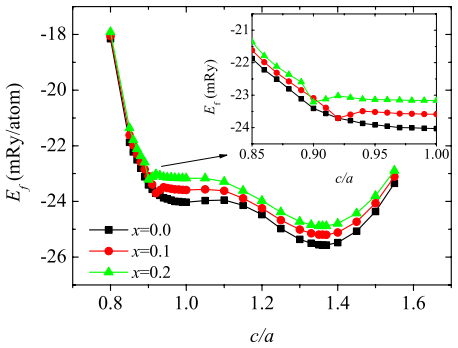

FIG. 3. (Color online) Theoretical formation energies of $Ni_{2+x}Mn_{1-x}Ga$ ($x=0$, 0.1, and 0.2) alloys as functions of the tetragonal c/a ratio. $c/a=1$ corresponds to the austenitic phase. Shown in the inset are the data points around $c/a=0.90$.

a shear modulus C' about half that calculated using the previous setup.[27] As a matter of fact, the present C' (7.9 GPa) is very close to that from plane-wave pseudopotential (PP) calculation (6.3 GPa)[20,49] as well as most experimental values (4.5 and 6.5 GPa).[51,53] The experimental C' (22 GPa) from Ref. 52 deviates significantly from the theoretical and other experimental values, which was ascribed by the authors to the slightly varied composition of the sample. The present bulk modulus and shear modulus C_{44} from Table I are in agreement with the experimental[1,51–53] as well as the previous first-principles[20,49,54] data. As expected, LSDA yields smaller lattice parameters (5.6563 Å) and larger bulk modulus (202.2 GPa) compared to those from GGA-PBE since LSDA generally overestimates the binding between the atoms.

B. Crystal structure

The equilibrium lattice constant of ferromagnetic $Ni_{2+x}Mn_{1-x}Ga$ with $L2_1$ crystal structure is shown in Fig. 2 as a function of the excess Ni concentration. Also shown are the lattice constants from experimental measurements.[28] The calculated lattice parameter decreases linearly with the excess Ni concentration. The x dependence of the theoretical lattice constant can be fitted as $a=5.2810-0.1081x$ (Å), which is in good agreement with the experimental relationship, $a=5.2845-0.1092x$ (Å). Note that the theoretical slope is only about 0.1% smaller than the experimental value.

The decrease in the lattice constant with increasing x may be attributed to two factors. One is that the atomic radius of the Ni (1.25 Å) is slightly smaller than that of Mn (1.27 Å). Therefore, the replacement of Mn by Ni induces the shrinkage of the crystal lattice. The other reason is the weakening of the magnetism of the system due to the substitution of Mn with Ni. Since an alloy in ferromagnetic state generally possesses a larger lattice parameter than in nonmagnetic state, the weakening of the magnetism with increasing Ni content in $Ni_{2+x}Mn_{1-x}Ga$ alloys results in a reduction in the lattice parameter.

For the martensite with nonmodulated tetragonal structure, we calculated the formation energy (E_f) with respect to the c/a ratio for each x. The E_f versus c/a curves for $x=0$, 0.1, and 0.2 are shown in Fig. 3. The formation energy of the alloy is defined as

$$E_f = E_{\text{tot}} - \frac{2+x}{4}E_{\text{Ni}} - \frac{1-x}{4}E_{\text{Mn}} - \frac{1}{4}E_{\text{Ga}} \tag{6}$$

with E_{tot} being the total energy per atom of the $Ni_{2+x}Mn_{1-x}Ga$ unit cell, and E_{Ni}, E_{Mn}, and E_{Ga} being the total energies per atom of fcc Ni, and Mn and Ga in a hypothetical fcc lattice.

It can be seen from Fig. 3 that, for $x=0$, two energy minima are found within the c/a range considered: one at $c/a=1$ corresponding to the $L2_1$ austenite and the other at $c/a=1.37$ corresponding to the experimentally observed nonmodulated β'''. The presence of the nonmodulated β' phase with $c/a<1$ is not seen in our total-energy curve. The absence of the nonmodulated phase in the stoichiometric Ni_2MnGa alloy is in agreement with the findings of Zayak *et al.*[54] and Godlevsky and Rabe[55] using pseudopotential plane-wave methods. Further investigations by Zayak and Entel[56] demonstrated that the β' phase may exist as five-layer modulated structure with $c/a \approx 0.95$.

For the nonmodulated β''' phase, the c/a from our calculations is larger than the experimental (1.18) and other theoretical (≈ 1.25) values.[1,10,28,54,55] This discrepancy we ascribe to the muffin-tin approximation employed in the present study. We note that the actual minimum in the total energy versus c/a sensitively depends on the basis set as well as on the potential sphere radii.[57,58] With *spd* basis set the theoretical equilibrium c/a of Ni_2MnGa is around 1.29 whereas *spdfg* yields $c/a \approx 1.37$. The conventional setup for the potential sphere radii (viz., $R_{mt}=R_{ws}$ for all sites) and *spd* basis set, on the other hand, predicts mechanically and thermodynamically unstable nonmodulated martensite.[57]

Before turning to the composition dependence of the calculated c/a, we would like to mention that quite a lot of efforts have been made to predict the equilibrium c/a ratio of the martensite by the use of first-principles methods.[54,55,59] However, it seems that this is a rather challenging task. Controversial results have been reported in the literature. For example, the $E(c/a)$ profile for perfect Ni_2MnGa calculated by Barman *et al.*,[59] using the full-potential linear-augmented

plane-wave method, differs significantly from that obtained in this study and those of Zayak *et al.*[54] and Godlevsky and Rabe.[55] Namely, the $E(c/a)$ profile by Barman *et al.*[59] shows a minimum at $c/a \approx 0.97$ but the deep minimum for β''' is completely absent.

For $x=0.1$ and 0.2, again, the β''' phase is found near $c/a \approx 1.37$. In the region with $c/a < 1$, we obtain a very shallow minimum at $c/a \approx 0.9$, corresponding to the nonmodulated β' phase. This suggests that the nonmodulated β' phase may occur as a metastable phase in $Ni_{2+x}Mn_{1-x}Ga$ alloys with high concentration of excess Ni. We note that the present c/a ratios of the nonmodulated β' phase are slightly smaller than the measured value (about 0.94).[1]

Comparing the $E_f(c/a)$ curves for different x, we find that, for $x=0$, there exists an observable energy barrier for the $L2_1$ to β''' transition at $c/a \approx 1.10$. This energy barrier almost vanishes for $x=0.1$ and $x=0.2$. On the other hand, from $x=0$ to $x=0.2$, the curves move up in the whole range of c/a. The formation energies become less negative, indicating that the replacement of Mn with Ni decreases the stability of the system.

The β' phase is only found for x larger than 0.06. This corresponds to the results of Zayak *et al.*[54] that the atomic disorder could stabilize the β'. According to the present results, for the β' phase c/a decreases almost linearly from 0.932 to 0.893 as going from $x=0.06$ to $x=0.2$. The decreasing c/a corresponds to increasing tetragonality of the β' phase, in line with the measurement of Lanska *et al.*[10] The increasing tetragonality has been related to the increasing T_M of the Ni-Mn-Ga based alloys.[10] However, for the nonmodulated β''' phase, the present c/a ratio remains almost unchanged with x. This result is against the powder x-ray diffraction measurements of Banik *et al.*[28] which showed that the c/a ratio of the β''' phase increases from about 1.18 to 1.23 with x increasing from 0.15 to 0.35. The reason for the discrepancy could be that the spherical constraint on the muffin-tin potential is not able to generate very accurate c/a ratio. However, since the main results from the present work do not explicitly use the theoretical c/a value, we believe that future improvement of the accuracy of the EMTO tool will not affect the present conclusions.

C. Phase stability and T_M

In order to get an idea of the connection between the experimental MT temperature and the relative stability of the austenite and martensite, we plot the formation energy difference between the austenite and martensite ($\Delta E_{AM}=E_f^{L2_1}-E_f^{\beta'''}$) as well as the measured T_M as functions of the concentration x of the excess Ni atoms in Fig. 4. As is shown in the figure, both ΔE_{AM} and T_M increase almost linearly with increasing x. The increasing ΔE_{AM} implies increasing stability of the β''' phase relative to the $L2_1$ phase. The ΔE_{AM} versus x and T_M versus x relationships can be fit as $\Delta E_{AM}(x)/\text{mRy} \approx 1.53+0.85x$ and $T_M(x)/\text{K} \approx 208+633x$, respectively, which for the ΔE_{AM} versus T_M relationship yields: $T_M/\text{K} \approx -931+744\Delta E_{AM}/\text{mRy}$. The correlation between ΔE_{AM} and T_M is expected, as ΔE_{AM} is the difference of thermodynamic potential between the high-temperature austenite and the low-temperature martensite phases.

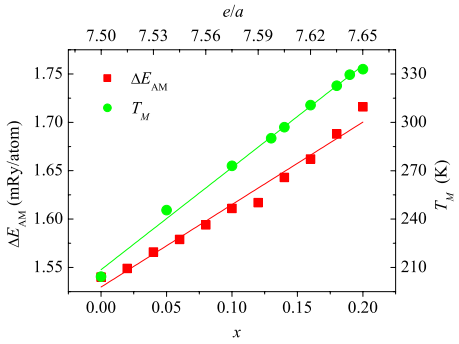

FIG. 4. (Color online) Theoretical formation energy difference between the $L2_1$ and β''' phases ($\Delta E_{AM}=E_f^{L2_1}-E_f^{\beta'''}$) and the experimental martensitic transition temperature (Ref. 2) T_M of $Ni_{2+x}Mn_{1-x}Ga$ ($x \leq 0.2$) alloys with respect to the concentration x (and e/a ratio, upper abscissa).

D. Elastic modulus and T_M

The calculated elastic constants of $Ni_{2+x}Mn_{1-x}Ga$ alloys ($x \leq 0.2$) in ferromagnetic $L2_1$ phase are listed in Table II. The bulk modulus B increases with increasing x (or e/a ratio) whereas C_{44} remains almost unchanged. The elastic constant C_{11} (C_{12}) decreases (increases) with x or e/a ratio, which results in softening the tetragonal elastic constant $C'=\frac{1}{2}(C_{11}-C_{12})$. For $x=0.2$, C' barely amounts to 1.6 ± 0.34 GPa, which indicates a marginal elastic stability toward a uniform tetragonal distortion.[20–22]

In Fig. 5, we plot C' and the measured T_M as a function of x and e/a. It is seen that C' decreases almost linearly with increasing x or e/a ratio, following the relationship $C'/\text{GPa} \approx 7.48-29.95x$ whereas T_M increases with x or e/a ratio, following $T_M/\text{K} \approx 208+633x$. Therefore, we may relate C' and T_M as $T_M/\text{K} \approx 366-21.14C'/\text{GPa}$. According to this, a larger C' corresponds to a lower T_M, in agreement with the correlation found for the other shape-memory alloys such as NiTi based alloys.[26]

The e/a ratio is a well-recognized predictor to determine qualitatively the composition dependent T_M.[10–12] For the $Ni_{2+x}Mn_{1-x}Ga$ alloy, we have $e/a=[10(2+x)+7(1-x)+3]/4=(30+3x)/4$. However, the $T_M \sim e/a$ ratio relationship is not guaranteed for some other off-stoichiometric Ni_2MnGa alloys. For examples, the substitution of the fourth elements such as Al and In to Ga (Refs. 13 and 14) and the variation in the long-range order of the $L2_1$ phase alter remarkably T_M (Refs. 15 and 16) but without changing e/a. From this point of view, C' as well as ΔE_{AM} could be better measures of the composition dependent T_M since both C' and ΔE_{AM} are expected to be sensitive to the composition (as well as the components) and long-range order as mentioned above. To confirm this assumption one should calculate the shear moduli and ΔE_{AM} of the $Ni_2Mn(GaAl)$ alloys and the Ni_2MnGa alloys with different long-range order.

E. Magnetic property and T_C

For $Ni_{2+x}Mn_{1-x}Ga$ alloys, it is found that the magnetic moment of the excess Ni atoms on the Mn sublattice (Ni_{Mn})

TABLE II. The elastic constants of $Ni_{2+x}Mn_{1-x}Ga(x \leq 0.2)$ alloys.

x	B (GPa)	C_{11} (GPa)	C_{12} (GPa)	C_{44} (GPa)	C' (GPa)	e/a
0.00	157.5 ± 0.60	168.0 ± 0.47	152.2 ± 0.23	107.0 ± 0.69	7.9 ± 0.35	7.500
0.02	157.8 ± 0.42	167.0 ± 0.51	153.2 ± 0.25	107.1 ± 3.46	6.9 ± 0.38	7.515
0.04	158.1 ± 0.32	166.2 ± 0.51	154.0 ± 0.25	107.2 ± 0.94	6.1 ± 0.38	7.530
0.06	158.5 ± 0.68	165.8 ± 0.47	154.9 ± 0.23	102.6 ± 2.39	5.4 ± 0.35	7.545
0.08	158.7 ± 0.36	165.3 ± 0.39	155.4 ± 0.19	110.0 ± 2.95	4.9 ± 0.29	7.560
0.10	159.0 ± 0.44	165.3 ± 0.36	155.9 ± 0.18	108.0 ± 0.44	4.7 ± 0.27	7.575
0.12	159.4 ± 0.50	164.3 ± 0.32	156.9 ± 0.16	108.4 ± 0.47	3.7 ± 0.24	7.590
0.14	159.8 ± 0.40	163.9 ± 0.31	157.8 ± 0.15	108.6 ± 0.50	3.1 ± 0.23	7.605
0.16	160.3 ± 0.12	163.9 ± 0.32	158.5 ± 0.16	108.9 ± 0.62	2.7 ± 0.24	7.620
0.18	160.5 ± 0.40	163.6 ± 0.41	159.0 ± 0.21	109.2 ± 1.29	2.3 ± 0.31	7.635
0.20	161.2 ± 0.46	163.3 ± 0.45	160.1 ± 0.23	109.0 ± 0.64	1.6 ± 0.34	7.650

is ferromagnetically coupled to those of the Ni atoms on the Ni sublattice (Ni_{Ni}) and the Mn atom on the Mn sublattice. The magnetic splitting of Ni_{Mn} is suppressed such that its magnetic moment is about half that of Ni_{Ni}. With increasing x, the magnetic moments of the Ni atoms decrease slightly whereas those of Mn and Ga remain almost unchanged. Since the magnetic moment of Ni atom is significantly smaller than that of the Mn atom, the total magnetic moment of $Ni_{2+x}Mn_{1-x}Ga$ decreases with increasing concentration of the excess Ni.

Several phenomenological models[17,29,30] have been presented to evaluate the Curie temperature T_C of magnetic materials, among which the simplest one is from Stoner, in which T_C is related to the energy difference between the nonmagnetic and the ferromagnetic states (ΔE_{NF}) by $T_C \approx \Delta E_{NF}/k_B$, with k_B being the Boltzmann constant.[17,29,30] Such a model has been employed to estimate T_C of the perfect Ni_2MnGa. However, the obtained T_C(≈3900 K) is more than ten times that from the experiments (376 K).[30] This finding is in agreement with the present calculation, where we get ΔE_{NF}=21.89 mRy/atom for Ni_2MnGa in the $L2_1$ structure, giving 3452 K for the transition temperature. The main reason behind the above discrepancy is that at high-temperature Ni_2MnGa has a paramagnetic state with nonvanishing disordered local magnetic moments.

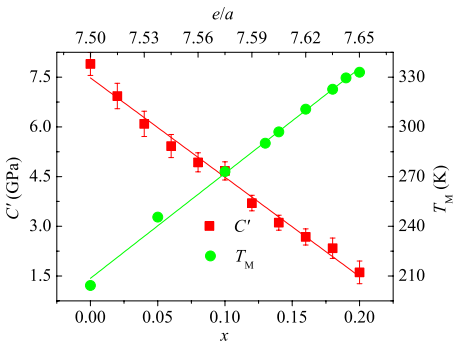

FIG. 5. (Color online) Theoretical shear modulus C' of the $L2_1$ phase (left ordinate) and the experimental martensitic transition temperature (Ref. 2) T_M (right ordinate) of $Ni_{2+x}Mn_{1-x}Ga(x \leq 0.2)$ alloys with respect to the concentration x (and e/a ratio, upper abscissa).

The disordered local magnetic-moment picture[31] offers a more realistic description of the PM state. Within the DLM, the $Ni_{2+x}Mn_{1-x}Ga$ system is described as a $(Ni^{\uparrow}_{Ni}Ni^{\downarrow}_{Ni})(Mn^{\uparrow}_{1-x/2}Mn^{\downarrow}_{1-x/2}Ni^{\uparrow}_{Mn,x/2}Ni^{\downarrow}_{Mn,x/2})Ga$ pseudoalloy, where the arrows mark the two spin states for Ni_{Ni}, Ni_{Mn}, and Mn. Using the PM state, the transformation temperature becomes $T_C \approx \Delta E_{PF}/S^{mag}$, where ΔE_{PF} is the energy difference between the PM (DLM) and FM states and $S^{mag} = \frac{1}{4}k_B\Sigma_i^4 c_i \ln(\mu_i+1)$ (μ_i is the magnetic moment and c_i the composition for site i) is the mean-field expression of the magnetic entropy valid for completely disordered local magnetic moment.[32] Our calculations give ΔE_{PF}=1.7 mRy for $L2_1$-Ni_2MnGa, which yields 724 K for the critical temperature of Ni_2MnGa. Thus although the transition temperature from Grimvall model is much lower than that from Stoner theory, it is still about twice of the experimental value. Recently, Şaşıoğlu *et al.*[35] have shown that the theoretical T_C of Heusler alloys can be significantly improved by using the Heisenberg Hamiltonian in combination with mean-field approximation. In the following, we adopt this approach to investigate the composition dependence of T_C of $Ni_{2+x}Mn_{1-x}Ga$ and compare the results with those obtained from the Grimvall model.

Figure 6 presents the effective exchange parameter of between Mn-Mn ($J_0^{Mn\text{-}Mn}$) and between Mn-Ni_{Ni} ($J_0^{Mn\text{-}Ni}$) as a function of the excess Ni concentration in $Ni_{2+x}Mn_{1-x}Ga(0 \leq x \leq 0.36)$ having the $L2_1$ and the β''' structures. The interaction parameters with Ni_{Mn} are small and thus they are not shown here. It is seen that, with increasing x, $J_0^{Mn\text{-}Mn}$ decreases for both crystallographic phases. However, the trend of $J_0^{Mn\text{-}Ni}$ is different: $J_0^{Mn\text{-}Ni}$ of the $L2_1$ phase first increases slightly and then decreases whereas that of the β''' always decreases with x increasing.

Figure 7 shows the composition dependence of the theoretical T_C for the $L2_1$ and β''' phases calculated from the Heisenberg model using the mean-field approximation [Eq. (5)]. For both phases, T_C decreases with increasing x. T_C of the β''' phase is higher than that of the $L2_1$ phase. The present theoretical T_C values are compared to the experimental data

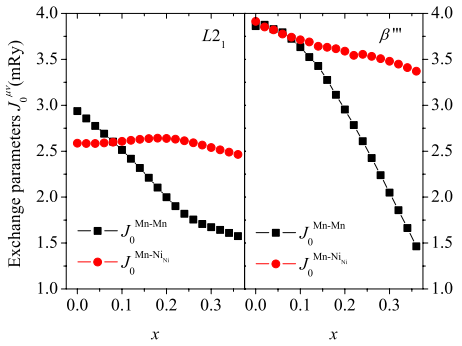

FIG. 6. (Color online) The effective exchange parameters $J_0^{\text{Mn-Mn}}$ (squares) and $J_0^{\text{Mn-Ni}}$ (circles) as a function of the excess Ni concentration x in $Ni_{2+x}Mn_{1-x}Ga$ ($0 \leq x \leq 0.36$) alloys. Results are shown for both $L2_1$ (left panel) and β''' (right panel) structures.

(also shown in Fig. 7). For $x < 0.18$, the experimental transition temperature decreases almost linearly with increasing x. However, for $x > 0.18$, the experimental T_C increases suddenly with increasing x. After reaching a maximum at about $x = 0.25$ it decreases again with x. This interesting experimental trend of T_C can be understood qualitatively from the present results. For $x < 0.18$, T_M is well below T_C so that the magnetic transition occurs in the $L2_1$ phase.[2] Therefore, the T_C of system corresponds to that of the $L2_1$ phase and decreases with increasing x, in line with the present finding. Since T_M increases whereas T_C decreases with increasing x, they become close to each other for $x \approx 0.18$.[2] Around this composition, the austenite and martensite phases may coexist and thus the measured T_C corresponds to a mixed rather than to a single phase. Since according to the present study the T_C of the martensite β''' phase is higher than that of the austenite $L2_1$ phase, it is understandable that the measured T_C goes up with increasing x, i.e., with increasing content of β''' phase in the system. When x exceeds 0.25, T_M becomes higher than T_C and the magnetic transition occurs within the β''' phase.[2] Therefore, the measured T_C corresponds solely to that of the martensite and decreases again with increasing x, in line with the present theory. We would like to point out the excellent agreement between the theoretical and experimental "jump" in T_C around $x \approx 0.18$ (Fig. 7).

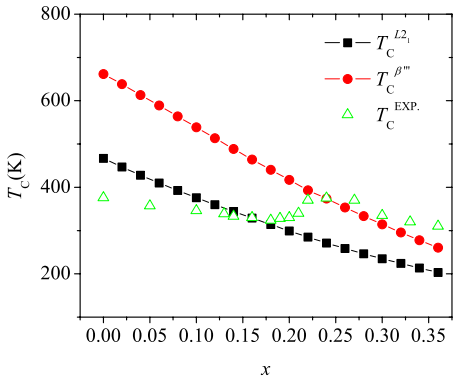

FIG. 7. (Color online) Theoretical T_C values as a function of the Ni concentration in $Ni_{2+x}Mn_{1-x}Ga$ ($0 \leq x \leq 0.36$) alloys. Results are shown for both $L2_1$ (squares) and β''' (spheres) structures. The experimental T_C values are from Ref. 2.

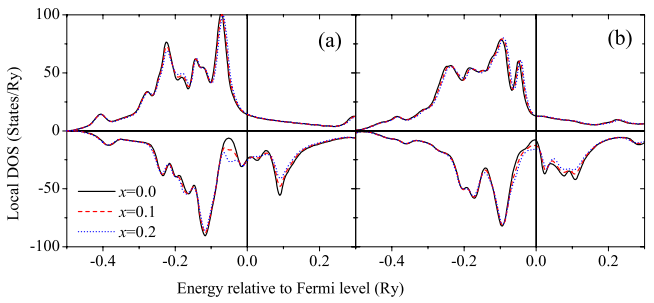

FIG. 8. (Color online) Total density of state of $Ni_{2+x}Mn_{1-x}Ga$ ($x = 0$, 0.1, and 0.2) alloys with $L2_1$ (panel a) and β''' (panel b) crystallographic structures. The vertical lines indicate the Fermi level. The minority (spin-down) density of states are represented in the lower part of each panel.

For comparison, the critical temperatures estimated from the Grimvall model adopting the PM-FM energy difference (not shown) follow the same linear trends as those obtained from the Heisenberg-MFA. For instance, for the $L2_1$ phase the $\Delta T_C/\Delta x$ slope of the Heisenberg-MFA T_C is −832 K. The corresponding slope from the Grimvall model is −794 K. Hence, although the Grimvall model fails to give accurate T_C values, it describes the composition dependence of $T_C(x)$ in line with the Heisenberg-MFA model. Note that the above theoretical slopes are larger than the average experimental slope[2] of −280 K calculated for $0 \leq x \leq 0.18$.

F. Electronic structure

In order to understand the atomistic origin of the composition dependence of the calculated physical parameters of $Ni_{2+x}Mn_{1-x}Ga$ alloys, we compare the total electronic density of states (DOS) and local DOS of $Ni_{2+x}Mn_{1-x}Ga$ with $x = 0$, 0.1, and 0.2 in Figs. 8 and 9.

As shown in Fig. 8, in the minority (spin-down) DOS of the $L2_1$ phase, there exists a pseudogap at about 0.05 Ry below the Fermi level, indicating the covalent bonding characters between the atoms in $Ni_{2+x}Mn_{1-x}Ga$. From Fig. 9, which shows the local DOS of Ni [(a) and (b)] and Ga [(e) and (f)], it is clear that the covalent bond is mainly formed due to the hybridization between the minority electronic states of Ni and Ga. As seen in Fig. 9, the resonance between the minority states of Ni and Ga around the pseudogap is more significant than that between Mn and Ga: the peak right below Fermi level of $L2_1$ phase is clearly seen in the local DOSs of both Ni [Fig. 9(a)] and Ga [Fig. 9(e)] but is not obvious for Mn [Fig. 9(c)]. This is understandable since Ni atom is the nearest neighbor whereas Mn is the second-nearest neighbor of Ga and, therefore, the interaction between Ni and Ga is expected to be stronger than that between Mn and Ga. The states below the pseudogap represent the bonding states whereas those above the pseudogap represent the antibonding states. Some of the antibonding states of the $L2_1$ phase are below the Fermi level, i.e., they are occupied by electrons. The occupation of antibonding states generally weakens the covalent bond. When the $L2_1$ phase transforms to β''', the pseudogap becomes wider and moves up in energy. In the β''' phase, the Fermi level locates right in the

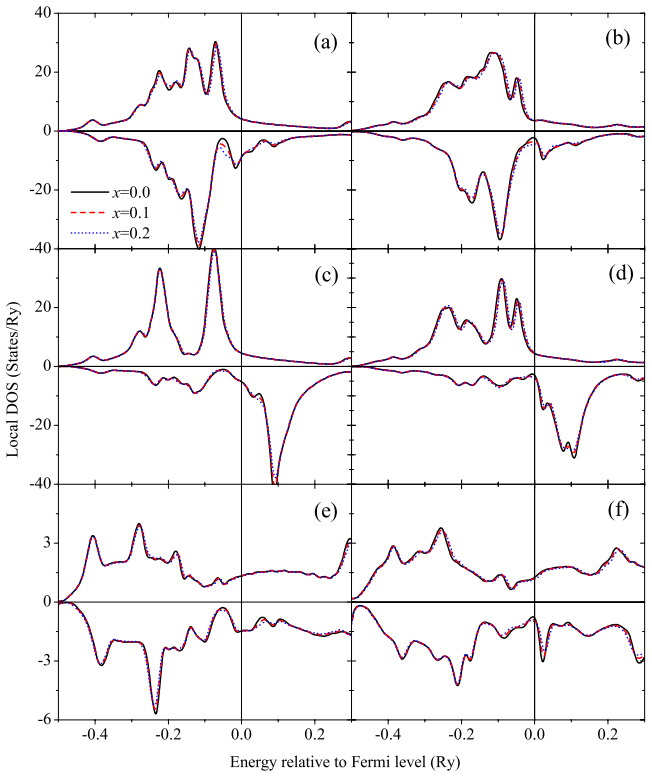

FIG. 9. (Color online) Local density of state of Ni (panels a and b) on Ni sublattice, Mn (panels c and d), Ga (panels e and f) in $Ni_{2+x}Mn_{1-x}Ga$ (x=0, 0.1, and 0.2) alloys with $L2_1$ (panels a, c, and e) and β''' (panels b, d, and f) crystallographic structures. The vertical lines indicate the Fermi level. The minority (spin-down) density of states is represented in the lower part of each panel.

valley of the pseudogap, i.e., the bonding states are fully occupied and the antibonding states are empty, indicating that the covalent bond in the β''' phase is stronger than that in the $L2_1$ phase. This is why the β''' phase is more stable than the $L2_1$ phase at ambient conditions. On the other hand, for the majority (spin-up) DOS, the state at about −0.05 Ry of the $L2_1$ phase splits when $L2_1$ phase transforms to β''' phase, which implies additional electronic interaction between the atoms in the β''' phase. This effect may also contribute to the improved stability of the β''' phase relative to the $L2_1$ phase. As seen from Figs. 9(a)–9(d), the splitting of the state at −0.05 Ry due to the $L2_1$ to β''' phase transition can mainly be ascribed to the electronic interaction between the Ni and Mn atoms.

With x increasing from 0 to 0.2, for both $L2_1$ and β''' phases, the pseudogap at about −0.05 Ry in the minority DOS becomes shallower (Fig. 8), which means that the covalent bond is weakened accordingly. This trend of the DOS is in agreement with the decreasing stability of the $L2_1$ and β''' phases with increasing x. Moreover, the increase in the minority DOS of Ni_{Ni} with increasing x [Fig. 9(a)] corresponds to the decreasing magnetic moments of the Ni_{Ni} atom as discussed at the beginning of Sec. III E.

IV. SUMMARY

In this paper, the concentration dependent properties of $Ni_{2+x}Mn_{1-x}Ga$ alloys and their relationship with the martensitic transition temperature T_M and Curie temperature T_C are investigated by the use of the first-principles EMTO-CPA method. The main results are summarized as follows: (1) for the austenite phase with $L2_1$ structure, the lattice constant decreases linearly with the concentration of the excess Ni atoms, x. At static conditions, the nonmodulated β''' phase is identified at $c/a \approx 1.37$ independent of the concentration x. For $x \geq 0.06$, the nonmodulated β' at $c/a < 1$ is found and the corresponding c/a ratio slightly decreases with increasing x. (2) The heats of formation of the $L2_1$ and β''' phases and their difference increase with increasing x, which indicates (a) decreasing lattice stability and (b) larger driving force for the $L2_1$-β''' martensitic phase transition, in accordance with the higher martensitic transition temperature T_M. (3) The shear modulus C' decreases with increasing x, which confirms that smaller C' corresponds to higher T_M. (4) With increasing x, the magnetic transition temperatures decrease for both $L2_1$ and β''' phases. For compositions where the two critical temperatures are close to each other, the magnetic transition temperatures of the austenite and martensite phases present, respectively, the lower and upper limits of the measured T_C of the alloy. (5) The covalent bond between minority spin states of Ni and Ga becomes weakened with increasing x, which accounts for the decreasing stability of the $Ni_{2+x}Mn_{1-x}Ga$ alloy with increasing x.

ACKNOWLEDGMENTS

The authors acknowledge the financial support from the MoST of China under Grant No. 2006CB605104 and from the NSFC under Grants No. 50871114 and No. 08-02-92201a (RFBR-NSFC project for the Sino-Russian cooperation). The Swedish Research Council, the Swedish Foundation for Strategic Research, the Swedish Energy Agency, and the Carl Tryggers Foundation are also acknowledged for financial support.

*Corresponding author; qmhu@imr.ac.cn

[1] P. J. Webster, K. R. A. Ziebeck, S. L. Town, and M. S. Peak, Philos. Mag. B **49**, 295 (1984).
[2] V. V. Khovaylo, V. D. Buchelnikov, R. Kainuma, V. V. Koledov, M. Ohtsuka, V. G. Shavrov, T. Takagi, S. V. Taskaev, and A. N. Vasiliev, Phys. Rev. B **72**, 224408 (2005).
[3] S. J. Murray, M. Marioni, S. M. Allen, R. C. O'Handley, and T. A. Lograsso, Appl. Phys. Lett. **77**, 886 (2000).
[4] A. Sozinov, A. A. Likhachev, N. Lanska, and K. Ullakko, Appl. Phys. Lett. **80**, 1746 (2002).
[5] J. Marcos, L. Mañosa, A. Planes, F. Casanova, X. Batlle, and A. Labarta, Phys. Rev. B **68**, 094401 (2003).
[6] A. N. Vasil'ev, V. D. Buchelnikov, T. Takagi, V. V. Khovailo, and E. I. Estrin, Usp. Fiziol. Nauk **173**, 577 (2003); Phys. Usp.

46, 559 (2003).
[7] X. Zhou, W. Li, H. P. Kunkel, and G. Williams, J. Phys.: Condens. Matter **16**, L39 (2004).
[8] C. Biswas, R. Rawat, and S. R. Barman, Appl. Phys. Lett. **86**, 202508 (2005).
[9] X. Jin, M. Marioni, D. Bono, S. M. Allen, R. C. O'Handley, and T. A. Lograsso, Appl. Phys. **91**, 8222 (2002).
[10] N. Lanska, O. Söderberg, A. Sozinov, Y. Ge, K. Ullakko, and V. K. Lindroos, J. Appl. Phys. **95**, 8074 (2004).
[11] A. T. Zayak, W. A. Adeagbo, P. Entel, and K. M. Rabe, Appl. Phys. Lett. **88**, 111903 (2006).
[12] T. Mehaddene, J. Neuhaus, W. Petry, K. Hradil, P. Bourges, and A. Hiess, Phys. Rev. B **78**, 104110 (2008).
[13] Y. Xin, Y. Li, C. B. Jiang, and H. B. Xu, Mater. Sci. Forum **475-479**, 1991 (2005).
[14] V. V. Kokorin, I. A. Osipenko, and T. V. Shirina, Phys. Met. Metallogr. **67**, 173 (1989).
[15] C. Seguí, J. Pons, and E. Cesari, Acta Mater. **55**, 1649 (2007).
[16] V. Sánchez-Alarcos, V. Recarte, J. I. Pérez-Landazábal, and G. J. Cuello, Acta Mater. **55**, 3883 (2007).
[17] A. Chakrabarti, C. Biswas, S. Banik, R. S. Dhaka, A. K. Shukla, and S. R. Barman, Phys. Rev. B **72**, 073103 (2005).
[18] J. Chen, Y. Li, J. X. Shang, and H. B. Xu, Appl. Phys. Lett. **89**, 231921 (2006).
[19] S. R. Barman, A. Chakrabarti, S. Singh, S. Banik, S. Bhardwaj, P. L. Paulose, B. A. Chalke, A. K. Panda, A. Mitra, and A. M. Awasthi, Phys. Rev. B **78**, 134406 (2008).
[20] C. Bungaro, K. M. Rabe, and A. Dal Corso, Phys. Rev. B **68**, 134104 (2003).
[21] M. Stipcich, L. Mañosa, A. Planes, M. Morin, J. Zarestky, T. Lograsso, and C. Stassis, Phys. Rev. B **70**, 054115 (2004).
[22] M. Wuttig, L. H. Liu, K. Tsuchiya, and R. D. James, J. Appl. Phys. **87**, 4707 (2000).
[23] X. Ren and K. Otsuka, Mater. Sci. Forum **327-328**, 429 (2000).
[24] X. Ren, K. Otsuka, and T. Suzuki, J. Alloys Compd. **355**, 196 (2003).
[25] K. Otsuka and X. Ren, Prog. Mater. Sci. **50**, 511 (2005).
[26] Q. M. Hu, R. Yang, J. M. Lu, L. Wang, B. Johansson, and L. Vitos, Phys. Rev. B **76**, 224201 (2007).
[27] Q. M. Hu, C. M. Li, R. Yang, S. E. Kulkova, D. I. Bazhanov, B. Johansson, and L. Vitos, Phys. Rev. B **79**, 144112 (2009).
[28] S. Banik, R. Ranjan, A. Chakrabarti, S. Bhardwaj, N. P. Lalla, A. M. Awasthi, V. Sathe, D. M. Phase, P. K. Mukhopadhyay, D. Pandey, and S. R. Barman, Phys. Rev. B **75**, 104107 (2007).
[29] S. Fujii, S. Ishida, and S. Asano, J. Phys. Soc. Jpn. **58**, 3657 (1989).
[30] O. I. Velikokhatnyi and I. I. Nuamov, Phys. Solid State **41**, 617 (1999).
[31] J. Staunton, B. L. Gyöffy, A. J. Pindor, G. M. Stocks, and H. Winter, J. Magn. Magn. Mater. **45**, 15 (1984).
[32] G. Grimvall, Phys. Rev. B **39**, 12300 (1989).
[33] M. Pajda, J. Kudrnovský, I. Turek, V. Drchal, and P. Bruno, Phys. Rev. B **64**, 174402 (2001).
[34] I. Turek, J. Kudrnovský, V. Drchal, and P. Bruno, Philos. Mag. **86**, 1713 (2006).
[35] E. Şaşıoğlu, L. M. Sandratskii, and P. Bruno, Phys. Rev. B **70**, 024427 (2004).
[36] R. M. Dreizler and E. K. U. Gross, *Density Functional Theory* (Springer, Berlin, 1998).
[37] L. Vitos, *Computational Quantum Mechanics for Materials Engineers* (Springer-Verlag, London, 2007).
[38] L. Vitos, Phys. Rev. B **64**, 014107 (2001).
[39] M. Zwierzycki and O. K. Andersen, Acta Phys. Pol. A **115**, 64 (2009).
[40] J. Kollár, L. Vitos, and H. L. Skriver, in *Electronic Structure and Physical Properties of Solids: The Uses of the LMTO Method*, Lectures Notes in Physics, edited by H. Dreyssé (Springer-Verlag, Berlin, 2000), p. 85.
[41] P. Soven, Phys. Rev. **156**, 809 (1967).
[42] B. L. Györffy, Phys. Rev. B **5**, 2382 (1972).
[43] L. Vitos, I. A. Abrikosov, and B. Johansson, Phys. Rev. Lett. **87**, 156401 (2001).
[44] J. P. Perdew, K. Burke, and M. Ernzerhof, Phys. Rev. Lett. **77**, 3865 (1996).
[45] J. P. Perdew and A. Zunger, Phys. Rev. B **23**, 5048 (1981).
[46] V. L. Moruzzi, J. F. Janak, and K. Schwarz, Phys. Rev. B **37**, 790 (1988).
[47] P. W. Anderson, in *Solid State Physics*, edited by F. Seitz and D. Turnbull (Academic Press, New York, 1963), Vol. 14, pp. 99–214.
[48] A. Liechtenstein, M. I. Katsnelson, and V. A. Gubanov, J. Phys. F: Met. Phys. **14**, L125 (1984); A. Liechtenstein, M. I. Katsnelson, V. P. Antropov, and V. A. Gubanov, J. Magn. Magn. Mater. **67**, 65 (1987).
[49] D. Chen, Q. M. Xiao, and Y. L. Zhao, B. H. Y, C. L. Wang, and D. H. Shi, Chin. Phys. Lett. **26**, 016201 (2009).
[50] A. Ayuela, J. Enkovaara, K. Ullakko, and R. M. Nieminen, J. Phys.: Condens. Matter **11**, 2017 (1999).
[51] J. Worgull, E. Petti, and J. Trivisonno, Phys. Rev. B **54**, 15695 (1996).
[52] L. Mañosa, A. Gonzàlez-Comas, E. Obradó, A. Planes, V. A. Chernenko, V. V. Kokorin, and E. Cesari, Phys. Rev. B **55**, 11068 (1997).
[53] T. E. Stenger and J. Trivisonno, Phys. Rev. B **57**, 2735 (1998).
[54] A. T. Zayak, P. Entel, J. Enkovaara, A. Ayuela, and R. M. Nieminen, J. Phys.: Condens. Matter **15**, 159 (2003).
[55] V. V. Godlevsky and K. M. Rabe, Phys. Rev. B **63**, 134407 (2001).
[56] A. T. Zayak and P. Entel, Mater. Sci. Eng., A **419-423**, 378 (2004).
[57] L. Vitos (unpublished).
[58] A. N. Vasil'ev, A. D. Bozhko, V. V. Khovailo, I. E. Dikshtein, V. G. Shavrov, V. D. Buchelnikov, M. Matsumoto, S. Suzuki, T. Takagi, and J. Tani, Phys. Rev. B **59**, 1113 (1999).
[59] S. R. Barman, S. Banik, and A. Chakrabarti, Phys. Rev. B **72**, 184410 (2005).